

Enhanced ionic conductivity and phase meta-stability of nano-sized thin film yttria-doped zirconia (YDZ)

WooChul Jung*, Joshua L. Hertz¹, Harry L. Tuller

Department of Materials Science and Engineering, Massachusetts Institute of Technology, Cambridge, MA 02139, USA

Received 28 August 2008; received in revised form 12 November 2008; accepted 12 November 2008

Available online 30 December 2008

Abstract

Yttria-doped zirconia (YDZ) thin films with nanometric sized grains were prepared by reactive RF sputtering and their oxygen ion conductivities were systematically measured as a function of yttria doping with levels in the range 0.5–9.1 mol.% Y_2O_3 . Enhanced oxygen ion conductivities, as derived from impedance spectra, were observed when compared with values reported for bulk YSZ. Furthermore, the peak conductivity for the YDZ films was observed to occur at considerably reduced yttria levels, i.e., at 6.5 mol.% Y_2O_3 (for $T > \sim 400$ °C) and at 3.2 mol.% Y_2O_3 (for $T < \sim 300$ °C) vs. 9 mol.% Y_2O_3 in bulk YSZ. Based on an analysis of the Raman spectra, these results are believed to result from the extended meta-stability of the cubic phase to reduced yttria levels at nanometric grain sizes. © 2008 Acta Materialia Inc. Published by Elsevier Ltd. All rights reserved.

Keywords: Yttria-doped zirconia (YDZ); Thin films; Impedance spectroscopy; Raman spectroscopy; Metastable phases

1. Introduction

Yttria-stabilized cubic zirconia (YSZ) is the best known and most investigated solid oxide ion conductor because of its high ionic conductivity coupled with chemical and mechanical stability over wide temperature and oxygen partial pressure limits [1]. This makes it particularly attractive for solid oxide fuel cell (SOFC) applications, where its resistance to reduction and oxidation ensures very low electronic conductivities and chemical expansion coefficients [2,3]. At very high-temperatures, pure zirconia (ZrO_2) has the cubic fluorite structure; upon cooling from its melting point (2680 °C), it transforms to the tetragonal form at 2370 °C and then to the monoclinic form at 1170 °C. The high-temperature structure can be stabilized to room temperature by substitution of larger cations of lower valence (e.g., Y^{3+}) for Zr^{4+} , which also introduces oxygen vacancies for charge compensation [4]. The fully stabilized cubic

phase, YSZ, is preferred as a SOFC electrolyte material given that it exhibits the highest ionic conductivity of the three phases and avoids phase-transformation-induced stresses and long-term ionic conductivity degradation characteristic of partially stabilized and unstabilized zirconia [5]. As a consequence, phase transformations in this system have been extensively studied for some time [6–9].

By far, the majority of experimental results have been obtained on high-temperature sintered bulk polycrystalline ceramics with micron-sized grains. On the other hand, detailed information regarding the phase stability of nanocrystalline YSZ thin films, prepared by low-temperature processes, remains limited [10–12]. From the standpoint of electrical characterization, the majority of studies on YSZ, even in thin film form, have focused mainly on 9–10 mol.% Y_2O_3 , known to exhibit the maximum ionic conductivity. Given the growing interest in thin film and micro SOFCs [13–18], a systematic approach toward understanding the relationship between composition, phase stability, and electrical properties in nanometric thin films is desirable and necessary. In this contribution, yttria-doped zirconia (YDZ) thin films, with systematically varying yttrium fraction, were prepared by reactive RF sputtering and their

* Corresponding author. Tel.: +1 617 253 2364; fax: +1 617 258 5749.
E-mail address: wjung@mit.edu (W. Jung).

¹ Present address: Department of Mechanical Engineering, University of Delaware, Newark, DE, USA.

electrical and structural properties were investigated by means of electrochemical impedance spectroscopy (EIS) and Raman spectroscopy, respectively.

2. Experimental

YDZ thin films, 1 μm thick and with a range of Y cation fraction, were deposited onto unheated fused silica substrates (surface temperatures reached $\approx 180^\circ\text{C}$ during deposition) by reactive RF magnetron sputtering (Kurt J. Lesker, Clairton, PA). Two-inch metal alloy targets with six different Zr to Y ratios ($\text{Zr}/\text{Y} = 99/1, 97/3, 94/6, 91/9, 88/12,$ and $84/16$), obtained from ACI Alloys (San Jose, CA), were used. The sputtering system was operated with a base pressure of 1×10^{-6} torr, a working pressure of 1×10^{-2} torr, and a RF plasma power of 200 W. Oxygen was introduced into the sputtering chamber at a ratio of 9:1 argon to oxygen to obtain oxide films.

The resulting films were characterized by transmission electron microscopy (TEM) and atomic force microscopy (AFM). The polycrystalline films were observed to have grain sizes between 30 and 50 nm (see Fig. 1). Chemical compositions, measured by wavelength dispersive X-ray spectroscopy (WDS) and X-ray photoelectron spectroscopy (XPS), exhibited good agreement, to within a few % error, with the cation composition of the corresponding target materials (see Table 1). Residual stresses induced in the films during heating and cooling the samples between room temperature and 450°C were measured with a Tencor 2320 wafer curvature measurement system (San Jose, CA). Raman spectroscopy (Kaiser Hololab 5000R Raman Spectrometer equipped with a Ti/S laser source of 785 nm wavelength) and X-ray diffraction (Rigaku RU300) were used to investigate the phases existing in the YDZ thin films.

For electrical measurements, dense interdigitated Pt microelectrodes of 100 nm thickness, prepared by DC sputtering and a photolithographic lift-off process were deposited onto the films (see Fig. 2). The finger width and inter-electrode spacings were 100 μm . A custom-designed enclosed probe station was used for the electrochemical impedance spectroscopy (EIS) measurements at temperatures between 230 and 500°C in air. The EIS measurements, covering the frequency range from 10 MHz to 0.01 Hz, with an AC amplitude of 30 mV, were performed with a Solartron 1260 impedance analyzer.

3. Results and discussion

Typical impedance results obtained from the YDZ thin films with interdigitated Pt electrodes exhibit three adjacent features, distinguished by a nearly ideal high-frequency semicircle, a more highly distorted intermediate frequency feature (see insert Fig. 3), and the beginnings of a much larger low frequency semicircle, normally attributed to the electrode impedance (see Fig. 3).

The high-frequency (HF) semicircle, attributed to YDZ grain conduction, is the focus of this study, given the inter-

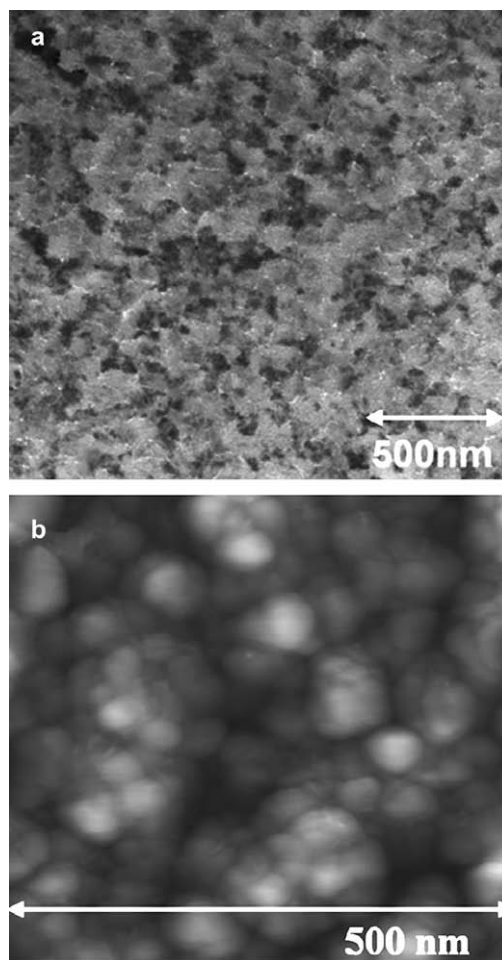


Fig. 1. (a) TEM and (b) AFM micrographs of YSZ thin films, indicating grain sizes on the order of 30–50 nm. The small white spots in the TEM micrograph result from over-etching during ion milling.

est in correlating grain composition with ionic conductivity. A distinct grain boundary contribution was not observed in this work. The absence of a grain boundary contribution is commonly observed in nanostructured thin films prepared by sputtering [19], pulsed laser deposition [20], evaporation [21], and solution-deposition [22]. Attempts to accommodate any distortions to the high-frequency semicircle by fitting a second semicircle never contributed to more than 10% of its total resistance. Due to the difficulty in isolating any grain boundary contribution, the diameter of the HF semicircle is henceforth used in calculating the grain conductivity. For a detailed discussion of how the impedance spectra of these thin film structures are analyzed, the reader is referred to a previous publication by the authors [23].

The resultant ionic conductivities for the films are plotted in Fig. 4 as $\log \sigma T$ versus reciprocal temperature. Except for films with 0.5 and 1.4 mol.% Y_2O_3 , all the YDZ films exhibit higher ionic conductivities than the relatively narrow band of conductivities reported for the most highly conductive bulk YSZ specimens, viz. that with ~ 9 mol.% Y_2O_3 . In Fig. 5, the ionic conductivities of the

Table 1

Compositional characterization of YDZ films focusing on the cation ratio (Y/Zr), as determined by WDS and XPS. (Note: the listed oxygen stoichiometries were estimated based on the measured Y/Zr ratios.)

| Technique | Target composition | Target Y/Zr ratio | Measured Y/Zr ratio | +/- | Estimated $Y_xZr_{1-x}O_{2-x/2}$ | Dopant level as % by oxide |
|-----------|---------------------|-------------------|---------------------|-------|----------------------------------|----------------------------|
| WDS | $Y_{0.01}Zr_{0.99}$ | 0.010 | 0.009 | 0.001 | $Y_{0.009}Zr_{0.991}O_{1.995}$ | 0.46 |
| | $Y_{0.03}Zr_{0.97}$ | 0.031 | 0.029 | 0.001 | $Y_{0.028}Zr_{0.972}O_{1.986}$ | 1.42 |
| | $Y_{0.06}Zr_{0.94}$ | 0.064 | 0.066 | 0.001 | $Y_{0.062}Zr_{0.938}O_{1.969}$ | 3.18 |
| | $Y_{0.09}Zr_{0.91}$ | 0.099 | 0.105 | 0.003 | $Y_{0.095}Zr_{0.905}O_{1.953}$ | 4.97 |
| | $Y_{0.16}Zr_{0.84}$ | 0.190 | 0.201 | 0.002 | $Y_{0.167}Zr_{0.833}O_{1.916}$ | 9.13 |
| XPS | $Y_{0.09}Zr_{0.91}$ | 0.099 | 0.097 | N/A | $Y_{0.088}Zr_{0.912}O_{1.956}$ | 4.62 |
| | $Y_{0.16}Zr_{0.84}$ | 0.190 | 0.189 | N/A | $Y_{0.159}Zr_{0.841}O_{1.921}$ | 8.63 |

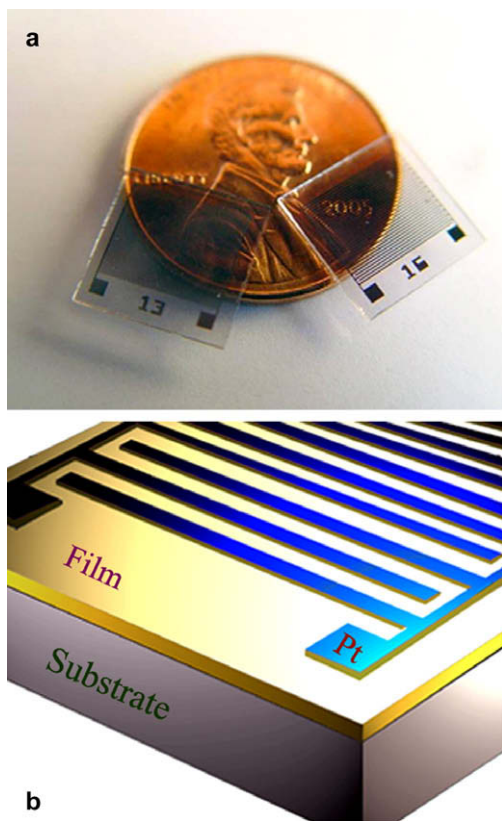


Fig. 2. Interdigitated electrode structures used for electrical characterization (a) photographed with a one-cent piece to indicate size, and (b) schematic view. Finger width and spacing were each 100 μm .

films measured at 500 $^{\circ}\text{C}$ (extracted from Fig. 4) are plotted as a function of mol.% Y_2O_3 . For a comparison, the ionic conductivities obtained from both single crystalline [24] and polycrystalline [25] YSZ samples are also inserted. Several key points should be noted. First, the maximum in film conductivity at this temperature falls at 6.5 mol.% Y_2O_3 rather than at 9 mol.% Y_2O_3 , normally found in bulk YDZ. Second, the magnitude of that conductivity is one order of magnitude greater than reported literature values for YSZ [24,25]. Lastly, even the 3.2 mol.% Y_2O_3 thin film specimen exceeds the ionic conductivity of that of the 9 mol.% Y_2O_3 thin film specimen, both of which exceed the bulk 9 mol.% Y_2O_3 . In Fig. 6, the corresponding activa-

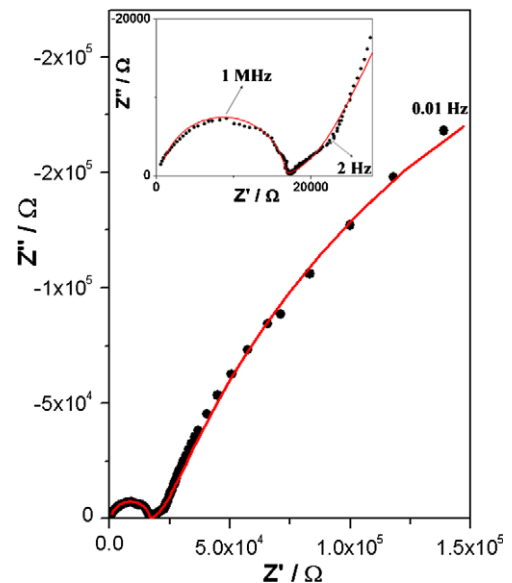


Fig. 3. A typical impedance spectrum for thin film YSZ deposited onto silica substrates. The measurement temperature was 390 $^{\circ}\text{C}$. Points are raw data; the line is the fit to the equivalent circuit.

tion energies associated with the conductivities reported in Fig. 5 for the thin films are plotted as a function of mol.% Y_2O_3 . The activation energy is observed to increase in a near linear fashion with increasing yttrium content from values close to 1.0 to 1.2 eV. As a consequence, at temperatures below about 300 $^{\circ}\text{C}$, the conductivity maximum shifts to the 3.2 mol.% Y_2O_3 composition.

Oxygen ion conduction in YSZ occurs via a vacancy mechanism, so an increase in acceptor concentration results in a larger vacancy concentration. However, clusters of ordered vacancies, with reduced mobility, form at high concentrations. The optimal concentration is presumably where the product of oxygen vacancy concentration and mobility leads to the highest conductivity. It is typically found at the composition corresponding to the tetragonal-cubic phase transition point [6]. However, the maximum conductivity could occur at lower yttrium content, due to reduced defect interactions, if the more highly symmetric cubic phase, usually characterized by higher mobility, could be stabilized.

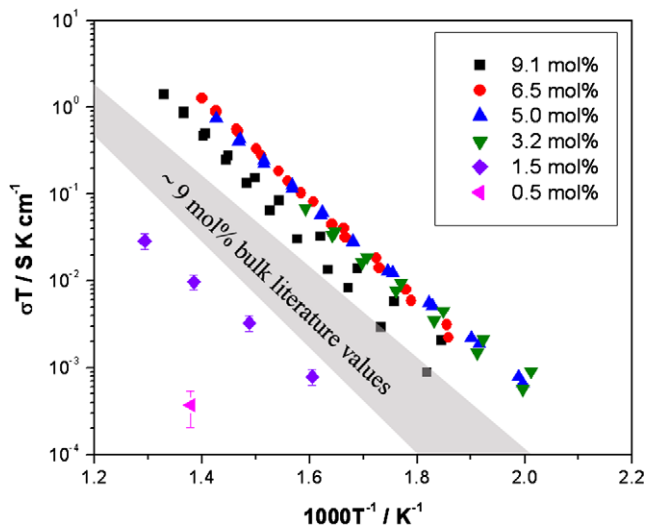


Fig. 4. Arrhenius plot of the ionic conductivity of various YSZ compositions, with 6.4 mol.% YSZ showing the highest conductivity at temperatures above about 400 °C. (Colored band indicates the bulk literature values [25,30–32], error bars were calculated based on the data fitting procedure. Some of error bars are not visible given their small magnitude.) (For interpretation of color mentioned in this figure the reader is referred to the web version of the article.)

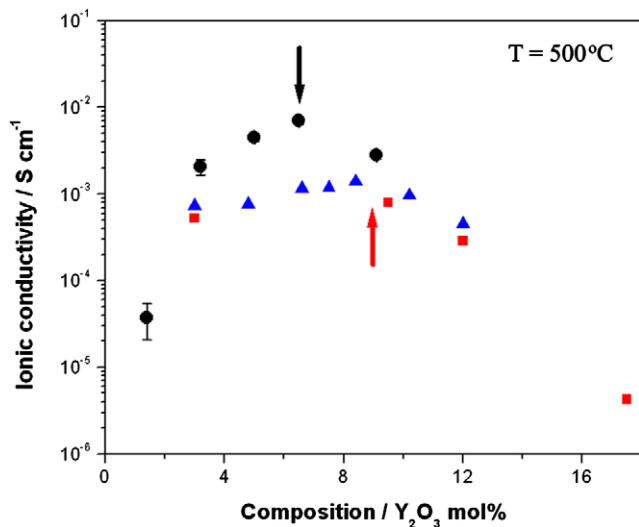


Fig. 5. Ionic conductivity vs. Y_2O_3 compositions of the YDZ thin film (solid circle) and the bulk YSZ ceramics (Ref. [25] (solid triangle) and Ref. [24] (solid square)) at 500 °C (arrows indicate peak positions).

While a minimum of $\sim 9\%$ Y_2O_3 is necessary to stabilize the cubic phase to reduced temperatures in bulk YSZ, we hypothesize that nanometric size grains, reduced deposition temperatures (180 °C) and/or substrate induced stresses may stabilize the cubic morphology at reduced doping levels, leading to reduced defect interactions.

The formation of metastable phases in nanostructured films has been reported repeatedly in the past. The tetragonal phase, stable only above 1200 K, exists at room temperature in undoped nanometric zirconia [27,28]. Several

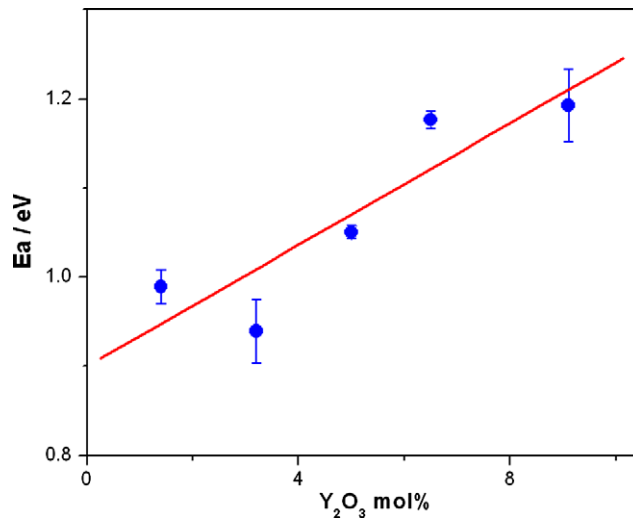


Fig. 6. Activation energy vs. Y_2O_3 compositions for the YDZ thin films. The activation energy is observed to increase nearly linearly with increasing yttrium content from values close to 1.0 to 1.2 eV.

metastable phases have been reported in sputter prepared YSZ films [10–12]. However, limited research, to date, has focused on the effects of nanocrystalline dimensions on the phase stability in YDZ electrolytes and their impact on transport properties.

In order to understand the source of enhanced conductivity in thin film YDZ, structural analysis was performed. Given the films' fine grain size and their very low thickness, deconvolution of the cubic and tetragonal phases could not be readily achieved by X-ray diffraction (see Fig. 7). On the other hand, Raman spectroscopy is better suited for identifying the phase boundary between the cubic and tetragonal phases, since a peak at $470\text{--}475\text{ cm}^{-1}$ exists only in the monoclinic and tetragonal phases, and not in the cubic phase [8,29]. In bulk YSZ, the intensity of this characteristic peak decreases with increasing Y_2O_3 content and reportedly disappears at higher than 9 mol.% Y_2O_3 [29]. The Raman spectra for all the specimens prepared in this study are presented in Fig. 8. While the 470 cm^{-1} peak is clearly visible from 0.5 mol.% up to 3.2 mol.% YDZ, it falls within the background noise level for values of 5.0 mol.% and above. Unfortunately, the high background signal emanating from the substrate makes it difficult to provide a quantitative analysis of the relative amounts of each phase. However, even considering the reduced resolution, the thin films in this work show very different Raman spectra compared with those reported for bulk YDZ where significant fractions of tetragonal and monoclinic phases can still be observed in 5.0 mol.% bulk YSZ [29]. The preliminary findings in this study are thus suggestive that a stabilized cubic morphology is achieved at considerably reduced yttria doping levels in thin film nanocrystalline zirconia.

The possible influence of residual stress on the conductivity of the thin films was also considered in this study. Stresses in films may come from a variety of sources including lattice and/or thermal expansion mismatch between film

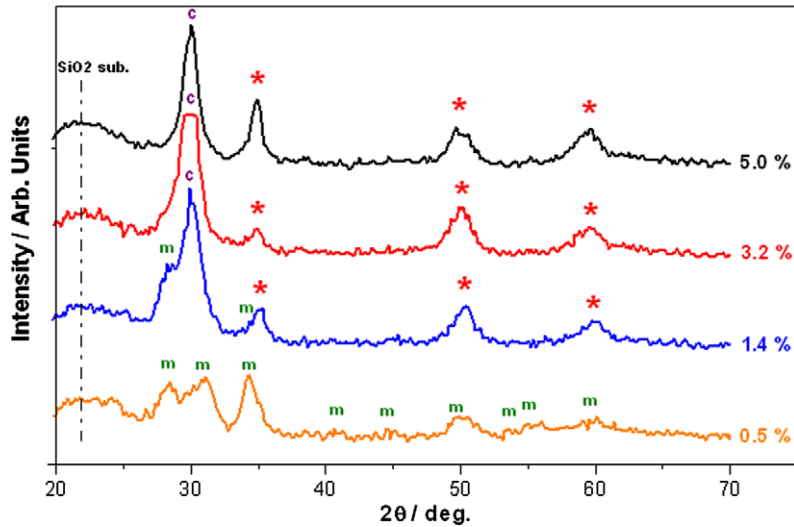


Fig. 7. XRD pattern of the YDZ thin films deposited on fused silica substrate. The symbol * indicates peaks where tetragonal and cubic phases are supposed to be distinguished by peak splitting. Given the films' fine grain size and their very low thickness, deconvolution of the cubic and tetragonal phases could not be achieved by XRD. Symbols c and m represent cubic/tetragonal peaks and monoclinic peaks, respectively. Concentration indicates Y₂O₃ mol.%.

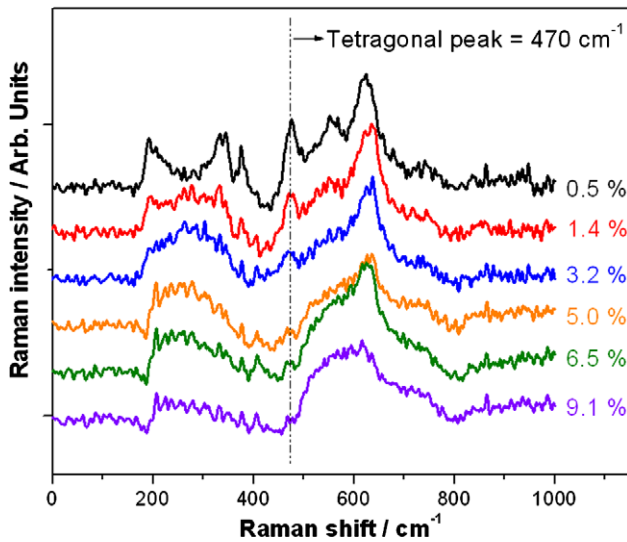


Fig. 8. Raman spectra of various YDZ compositions, showing peak locations of monoclinic/tetragonal (470 cm⁻¹). Concentration indicates Y₂O₃ mol.%.

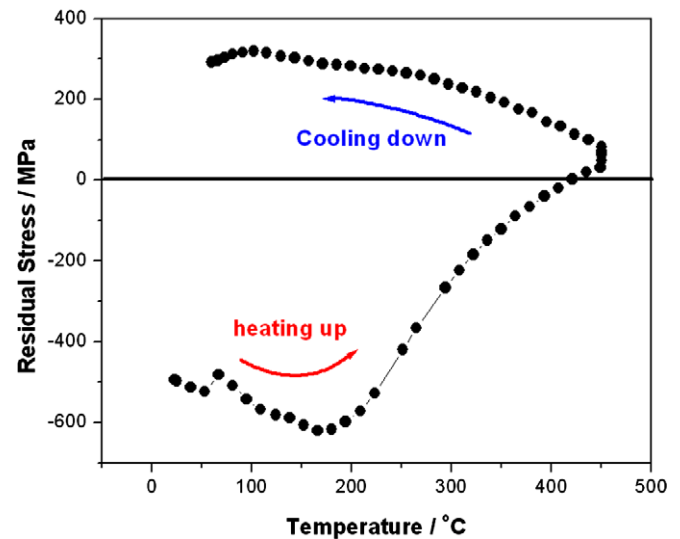


Fig. 9. Total residual stress vs. temperature during post-deposition thermal cycles for a sputtered 9 mol.% YDZ film deposited onto a fused silica substrate.

and substrate and, in particular, for sputtered films, from ion bombardment damage during deposition. 5 mol.% YDZ films, grown by the authors by reactive sputtering under identical conditions onto Si single crystal wafers, were previously reported to exhibit substantial compressive stresses [26]. During post-annealing, with increasing temperature, the compressive stress decreased and ultimately switched from compressive to tensile at approximately 450 °C. Subsequent heating and cooling cycles closely followed the cooling curve. Similar residual stress measurements were conducted in the present study on 1- μ m thick YDZ films sputtered onto a fused silica substrate. The

results, shown in Fig. 9, show a similar trend to that observed previously on YSZ films grown on Si [26]. Electrical conductivity measurements performed on films following the same heating and cooling cycles over the temperature range of interest demonstrated no distinct hysteresis phenomena even while the residual stress varied markedly from compressive to tensile. Further, according to Ref. [26], the compressive stress of the sputtered YDZ films largely relaxes above a thickness of 300 nm even without heating, as confirmed in this work. Therefore, one can confidently conclude that residual stresses do not have a significant impact on the conductivity results in this study.

4. Conclusion

YDZ thin films with nanometric grains were prepared by reactive RF sputtering, and enhanced ionic conductivity at considerably reduced yttria doping levels, compared with bulk YSZ, were found. Based on Raman spectroscopy measurements, the existence of a metastable cubic phase at reduced yttrium levels is suggested. Our results, to date, demonstrate that nanocrystalline YDZ thin films, at low Y content, show unexpected enhancements in transport properties as compared to the microcrystalline bulk state. Stress effects appear to play, at most, a secondary role in impacting the ionic conductivity. Further examination of these surprising results may shed new light on other phenomena deriving from the nanocrystalline and/or thin film character of YDZ as well as the potential for enhanced electrical and electrochemical properties.

Acknowledgements

This work was supported by the National Science Foundation material world network collaboration under Grant No. DMR-0243993. This work made use of the Shared Experimental Facilities supported by the MIT MRSEC Program of the National Science Foundation under Grant No. DMR 02-13282 and the MIT Microsystems Technology Laboratories. The authors thank Prof. S. Reich, Freie Univ. and Z.I. Kalcioğlu, MIT for assisting with the Raman data analysis. The authors also thank the Samsung Scholarship for financial support.

References

- [1] Steele BCH. *J Power Sources* 1994;49:1.
- [2] Yokokawa H, Sakai N, Horita T, Yamaji K, Brito ME. *MRS Bull* 2005;30:591.
- [3] Atkinson A, Ramos TMGM. *Solid State Ionics* 2000;129:259.
- [4] Goodenough JB. *Ann Rev Mater Res* 2003;33:91.
- [5] Butz B, Kruse P, Störmer H, Gerthsen D, Müller A, Weber A, et al. *Solid State Ionics* 2006;177:3275.
- [6] Hull S. *Rep Prog Phys* 2004;67:1233.
- [7] Scott HG. *J Mater Sci* 1975;10:1527.
- [8] Yashima M, Kakihana M, Yoshimura M. *Solid State Ionics* 1996;86–8:1131.
- [9] Yoshimura M. *Am Ceram Soc Bull* 1988;67:1950.
- [10] Hobein B, Tietz F, Stover D, Cekada M, Panjan P. *J Eur Ceram Soc* 2001;21:1843.
- [11] Jankowski AF, Hayes JP. *Surf Coat Technol* 1995;76:126.
- [12] Kao AS. *J Appl Phys* 1991;69:3309.
- [13] Baertsch CD, Jensen KF, Hertz JL, Tuller HL, Vengallatore ST, Spearing SM, et al. *J Mater Res* 2004;19:2604.
- [14] Bieberle-Hutter A, Beckel D, Infortuna A, Muecke UP, Rupp JLM, Gauckler LJ, et al. *J Power Sources* 2008;177:123.
- [15] Hertz JL, Rothschild A, Tuller HL. *J Electroceram* 2008. doi: [10.1007/s10832-008-9475-5](https://doi.org/10.1007/s10832-008-9475-5).
- [16] Hertz JL, Tuller HL. *J Electrochem Soc* 2007;154:B413.
- [17] Litzelman SJ, Hertz JL, Jung W, Tuller HL. *Fuel Cells* 2008;8:294.
- [18] Shao ZP, Haile SM, Ahn J, Ronney PD, Zhan ZL, Barnett SA. *Nature* 2005;435:795.
- [19] Thiele ES, Wang LS, Mason TO, Barnett SA. *J Vac Sci Technol A Vac Surf Films* 1991;9:3054.
- [20] Joo JH, Choi GM. *Solid State Ionics* 2006;177:1053.
- [21] Hartmanova M, Thurzo I, Jergel M, Bartos J, Kadlec F, Zelezny V, et al. *J Mater Sci* 1998;33:969.
- [22] Chen CC, Nasrallah MM, Anderson HU. *Synthesis and characterization of Ysz thin-film electrolytes*. Elsevier Science Bv; 1994. p. 101.
- [23] Hertz JL, Tuller HL. *Solid State Ionics* 2007;178:915.
- [24] Filal M, Petot C, Mokchah M, Chateau C, Carpentier JL. *Solid State Ionics* 1995;80:27.
- [25] Luo J, Almond DP, Stevens R. *J Am Ceram Soc* 2000;83:1703.
- [26] Quinn DJ, Wardle B, Spearing SM. *J Mater Res* 2008;23:609.
- [27] Baldinozzi G, Simeone D, Gosset D, Dutheil M. *Phys Rev Lett* 2003;90:4.
- [28] Djurado E, Bouvier P, Lucazeau G. *J Solid State Chem* 2000;149:399.
- [29] Yashima M, Ohtake K, Arashi H, Kakihana M, Yoshimura M. *J Appl Phys* 1993;74:7603.
- [30] Abelard P, Baumard JF. *Phys Rev B* 1982;26:1005.
- [31] Manning PS, Sirman JD, DeSouza RA, Kilner JA. *Solid State Ionics* 1997;100:1.
- [32] Park JH, Blumenthal RN. *J Electrochem Soc* 1989;136:2867.